Batteries & Supercaps

Research Article
doi.org/10.1002/batt.202500239

Chemistry Europe
European Chemical Societies Publishing

www.batteries-supercaps.org

Effects of Fluorinated Additives in Molten Salt Electrolytes for Calcium Batteries

Carolina Cruz and Patrik Johansson*

Fluorinated additives offer a promising route to tailor the structure and transport properties of electrolytes in general, yet their role in molten salt electrolytes (MSEs) remains poorly understood. Here, the influence of three fluorinated additives, 1,1,2,2-tetrafluoroethyl-2,2,3,3-tetrafluoropropyl ether (TTE), 1,2- bis(2,2,2-trifluoroethoxy) ethane (BTFE), and PhF, on the structure and dynamics of an MSE composed of [Li, Na, K, Ca]FSI, is investigated using molecular dynamics simulations—with the end-goal of improved calcium battery (CaB) electrolytes. The differences in additive chemical structure affect cation coordination, ionic cage persistence, and ligand exchange kinetics; while TTE and BTFE directly participate in cation coordination, PhF acts as a non-coordinating diluent, weakening the ionic network through spatial disruption. These additive-specific effects result in cation-dependent trends in coordination and mobility. Overall, the findings provide a proof-of-concept for rational additive selection in MSEs, shifting the design paradigm from optimizing bulk conductivity toward engineering coordination and interfacial behavior for CaB electrolytes.

1. Introduction

The increasing demand for efficient energy storage has placed significant pressure on lithium-ion battery (LIB) technology, raising concerns regarding materials availability, supply risks, and sustainability.[1–3] As a result, research has increasingly focused on next-generation battery (NGB) alternatives based on more abundant and cost-effective materials.[2,4,5] Within this group, multivalent battery chemistries offer the advantage of transferring multiple charges per ion, enabling larger charge storage capacities and possibly energy densities.[5–7] Among these, calcium batteries (CaBs) have gained attention due to their balance of natural abundance, low cost, and high volumetric capacity when metal anodes are employed.[3,8] However, alongside these advantages, developing efficient electrolytes for CaBs remains a major challenge, in particular, to achieve high ionic conductivity and stable calcium plating/stripping under practical conditions.[9–11]

Molten salt electrolytes (MSEs) have been proposed as a viable solution to these challenges due to their inherent thermal and electrochemical stability.[12–14] The transport properties and electrochemical performance of MSEs are governed by the interplay between cationic and anionic species. Among the anions used in MSEs for battery applications, bis(fluorosulfonyl)imide (FSI) is particularly notable for offering high ionic conductivity and low melting points, making them more suitable for operation in ambient to elevated temperature conditions as compared to their bis(trifluoromethanesulfonyl)imide (TFSI) counterparts, mainly due to its smaller size, which reduces steric hindrance and facilitates ion transport.[15–17] On the cation side, alkali and alkaline-earth metals such as lithium (Li^+), sodium (Na^+), potassium (K^+), and calcium (Ca^{2+}) strongly influence the MSE structure and dynamics,[18–20] but a common denominator is high viscosity, impeding the ion transport at lower temperatures.[21,22]

To address these limitations, additives, co-solvents, or diluents are often introduced. Fluorinated diluents, such as 1,1,2,2-tetrafluoroethyl-2,2,3,3-tetrafluoropropyl ether (TTE) and bis(2,2,2-trifluoroethyl) ether (TFEE), have for long been considered inert, that is, not directly interacting with the ionic species, in particular in LIB electrolytes, affecting only macroscopic properties, such as viscosity and conductivity.[23,24] Recent studies, however, challenge this assumption, demonstrating a direct impact on the cation solvation, and thus they are, sometimes, rather additives or co-solvents (depending on the percentage added).[25,26]

For instance, Ishfaq et al.[25] reported that the cyclic fluorinated ether 2,2-bis(trifluoromethyl)-1,3-dioxolane (BTFD) does not coordinate directly with lithium ions but instead shifts the solvation structure by promoting lithium-anion coordination, which influences interphase formation and battery performance. Similarly, Ekeren et al.[27] reported that TFEE weakens cation–anion interactions in localized highly concentrated electrolytes (LHCEs), enhancing ionic conductivity while maintaining the structural integrity of solvation clusters. Furthermore, Jia

C. Cruz, P. Johansson
Department of Physics
Chalmers University of Technology
412 96 Göteborg, Sweden
E-mail: patrik.johansson@chalmers.se

P. Johansson
Alistore-ERI
CNRS FR 3104
15 Rue Baudelocque, 80039 Amiens, France

P. Johansson
Department of Chemistry– Ångström
Uppsala University
SE-751 21 Uppsala, Sweden

Research Article
doi.org/10.1002/batt.202500239
Chemistry Europe
European Chemical Societies Publishing

et al.[26] investigated TTE and found that it does not directly coordinate with lithium ions. Instead, TTE facilitates the formation of ionic aggregates by acting as a non-coordinating medium.

On the contrary, some fluorinated additives exhibit weak yet direct interactions with cations and thus act as (co-)solvents. Perez Beltran et al.[23] investigated the role of TTE in the solvation and coordination environment of Li^+ within LHCEs and found that TTE interacts with Li^+ primarily through its fluorine atoms rather than via its oxygen atoms, and this interaction partially disrupts the coordination by dimethyl carbonate (DMC). The Li^+–$F_{(TTE)}$ interactions are, however, weaker than the Li^+–$O_{(DMC)}$ and Li^+–$O_{(FSI)}$ interactions, making them more transient than stable. These findings suggest that TTE is not entirely inert in LHCEs and highlight the importance of subtle molecular interactions.

Overall, the above illustrates the nuanced role of fluorinated solvents in electrolytes, underscores the complexity, and highlights the need for further research to disentangle the effects of solvent chemistry, concentration, and electrolyte composition, particularly in MSEs.

Additionally, fluorinated solvents have, as mentioned earlier, been shown to influence interfacial properties, both solid electrolyte interphases (SEIs) and cathode electrolyte interphases (CEIs) by facilitating the formation of robust, mechanically stable layers rich in LiF or other fluorine-containing compounds, contributing to improved cycling stability and reduced electrolyte degradation.[28,29]

The role of fluorinated solvents in NGB and especially CaB electrolytes, however, remains more or less unexplored.[30–33] The use of fluorinated solvents as additives in MSEs for CaBs may differ from their use in LIB electrolytes, where they are mere diluents, that is, not taking part in the cation solvation, to actively solvate and stabilize ionic interactions.[34,35]

Here, we elucidate the roles of three different fluorinated solvents: TTE, 1,2- bis(2,2,2-trifluoroethoxy) ethane (BTFE), and fluorobenzene (PhF), all employed in equimolar quaternary MSEs of [Li, Na, K, Ca]FSI (**Figure 1**). We use molecular dynamics (MD) simulations to analyze, in particular, the (cation) solvation, ionic cage dynamics, and transport properties. The [Li, Na, K, Ca]FSI MSE, without any added solvent, previously studied by us,[12] serves as a reference point for all properties studied. While this work focuses on the structural and dynamic effects of fluorinated additives in the bulk phase, it does not address their electrochemical stability or decomposition under applied potentials. Fluorinated solvents such as BTFE have been shown to undergo reductive degradation during cycling, generating species like HF that can compromise SEI integrity and long-term performance.[36,37] Therefore, additive selection must ultimately balance solvation function with chemical stability, a trade-off that warrants further investigation through complementary interfacial modeling and experimental studies.

2. Results and Discussion

We begin by analyzing the local structure of the MSEs through RDFs and CNs for cation coordination and the effects of the additives/co-solvents. Subsequently, we analyze the different energetic contributions in terms of Coulombic, vdW, and potential energies.

Finally, we analyze the dynamics, via MSDs and self-diffusion coefficients, ligand exchange rates (LERs), and cage lifetimes (CaLs).

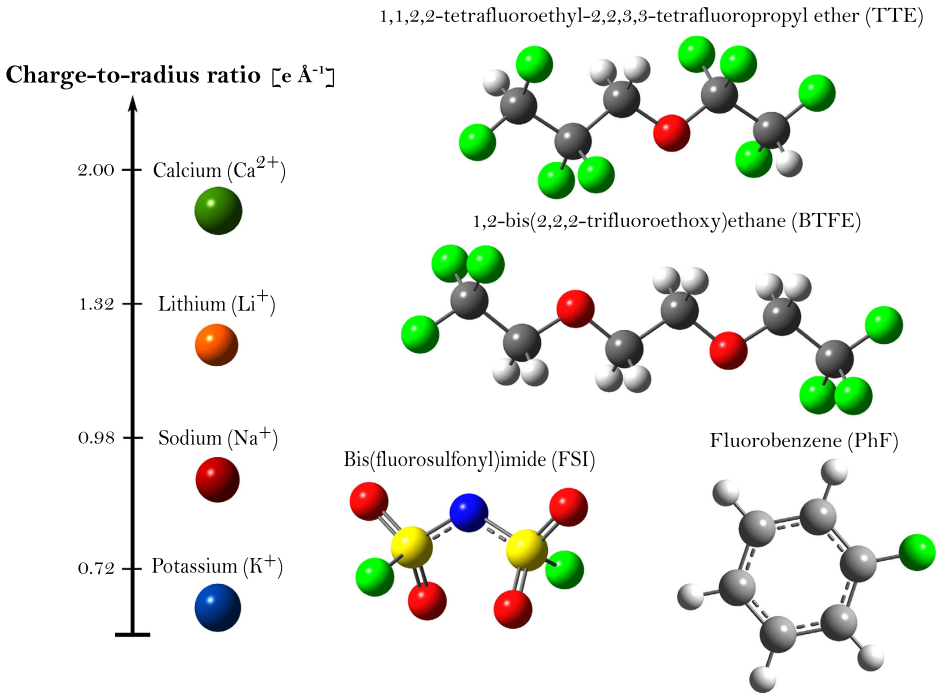

Figure 1. Comparison of charge-to-radius ratios for Li^+, Na^+, K^+, and Ca^{2+} cations (left), alongside the chemical structures of the FSI anion, and the TTE, BTFE, and PhF solvents (right).

Research Article
doi.org/10.1002/batt.202500239
Chemistry Europe
European Chemical Societies Publishing

2.1. Local Structure

The local structure analysis using RDFs for cation–oxygen ($M^{+/2+}$-O) interactions reveals a prominent peak within the range 1.8 Å < r < 3.0 Å across all MSEs (**Figure 2**-a, d, g, j), indicative of strong cation coordination by the oxygen atoms from the anions. Beyond this range, the RDFs converge to unity, consistent with liquid-phase behavior. For cation–nitrogen ($M^{+/2+}$-N) interactions, a weaker peak appears within the same radial range (Figure 2-b, e, h, k), followed by a second, more pronounced peak between 3.5 Å < r < 5.0 Å, which decays at longer distances. Since the primary coordination shell is dominated by oxygen from the anions and no secondary peak is observed in the $M^{+/2+}$-O RDFs, this second peak in the $M^{+/2+}$-N RDFs likely arise due to geometric constraints imposed by $M^{+/2+}$-O coordination and the anion structure rather than representing a distinct coordination shell.

In the TTE- and BTFE-based MSEs, the RDFs show small, yet noticeable, peaks corresponding to cation–oxygen interactions from the fluorinated additives/solvents within the range 1.8 Å < r < 3.0 Å (Figure 2-d, g). This suggests that TTE and BTFE are not merely passive spectators but do participate in the first cation coordination shell, albeit to a minor extent, as observed for TTE by Perez Beltran et al. for LiFSI in localized high-concentration electrolytes.[23] However, recent molecular dynamics simulations by Ishfaq et al. show that BTFE remains largely excluded from the Li^+ solvation shell, with no significant Li–O(BTFE) coordination peak, indicating that its influence is primarily indirect.[25] To date, there is no conclusive evidence that BTFE directly participates in the cation coordination shell. In contrast, the PhF-based MSE exhibits no discernible RDF peak within the first cation coordination shell (Figure 2-j), showcasing that PhF remains a true spectator. The non-solvating nature of PhF as a diluent was also reported by Jiang et al. for a highly concentrated LiFSI/DMC electrolyte, where Raman spectroscopy indicated no direct involvement of PhF in the Li^+ coordination shell. Instead, PhF contributed to the formation of a LiF-rich SEI.[38] Additionally, Li et al. reported that PhF acts as a non-coordinating diluent, modifying the dielectric environment of the $LiPF_6$/FEC/EMC electrolyte without participating directly in Li^+ coordination.[24] In the pure FSI, TTE- and BTFE-based MSE, there are $M^{+/2+}$-F features at longer distances, indicating weak interactions and/or being simple geometric consequences of the stronger interactions (Figure 2-c, f, i).

The trends observed in the RDFs are further supported by the CN analysis (**Figure 3**). In general, the CNs ($M^{+/2+}$-O, $M^{+/2+}$-N, and total) decrease for Li^+, Na^+, and K^+ in the presence of fluorinated additives as compared to the pure FSI-based MSE. This decrease reflects less densely packed first cation coordination shells. In contrast, Ca^{2+} maintains a consistently high CN across all MSEs, suggesting that its coordination remains unaffected, mainly due to strong Coulombic interactions. This behavior aligns with the

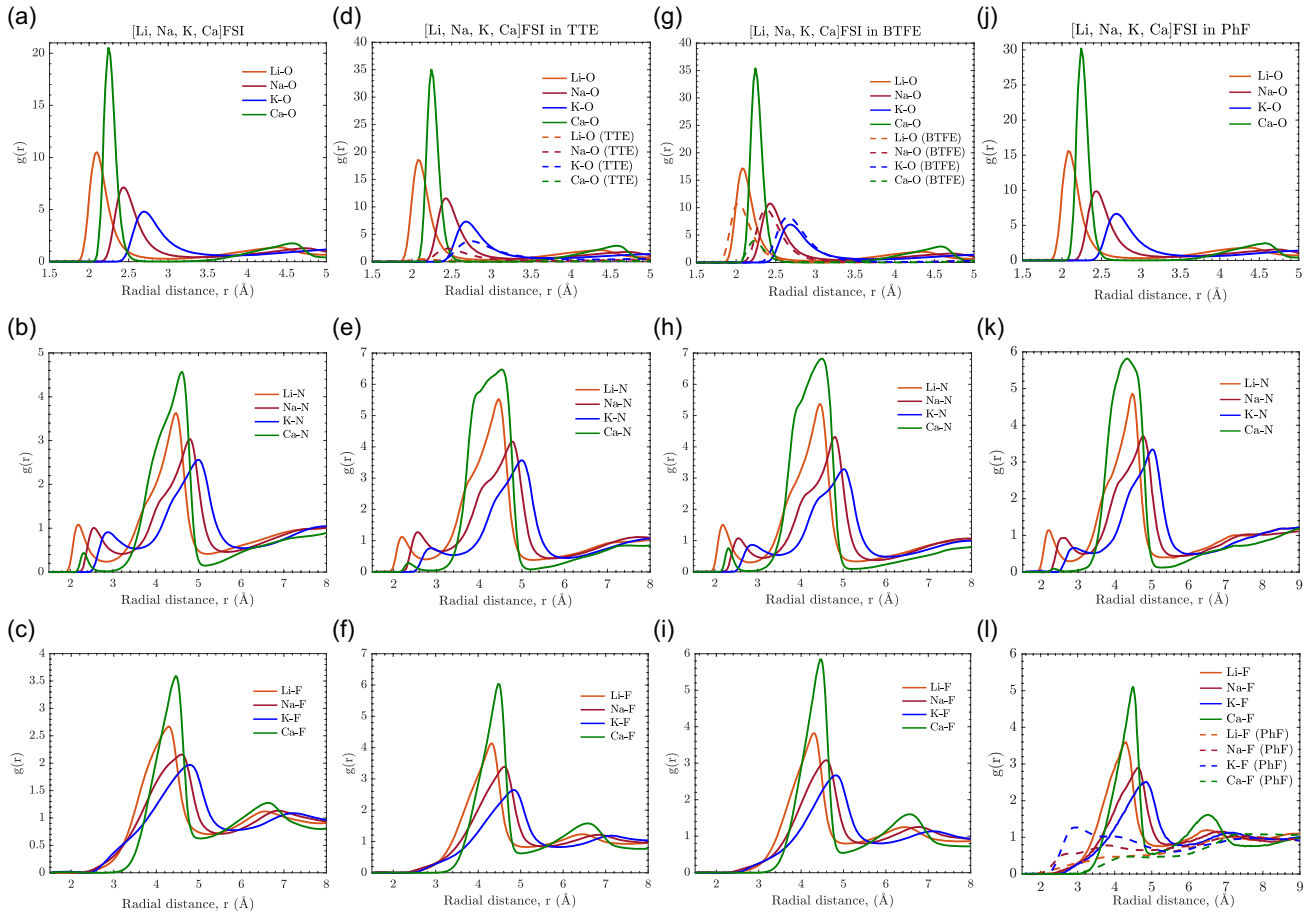

Figure 2. RDFs for $M^{+/2+}$-O, $M^{+/2+}$-N, and $M^{+/2+}$-F interactions in FSI- a–c) FSI-TTE- d–f), FSI-BTFE g–i), and FSI-PhF-based j–l) MSEs.

Research Article
doi.org/10.1002/batt.202500239
Chemistry Europe
European Chemical Societies Publishing

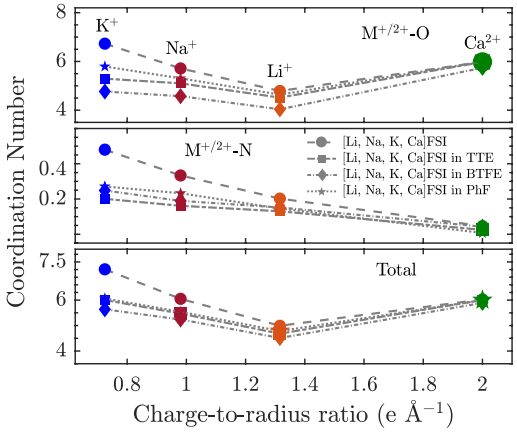

Figure 3. pCNs for $M^{+/2+}$-O (top) and $M^{+/2+}$-N (middle), and CNs (bottom) for Li^+, Na^+, K^+, and Ca^{2+} in FSI-, FSI-TTE-, FSI-BTFE-, and FSI-PhF-based MSEs.

findings of Biria et al. who reported consistently high CNs for Ca^{2+}, ≈6 to 8, across a range of solvents (EC, DMC, PC, and ionic liquids).[35]

Overall, the BTFE-based MSE exhibits the lowest CNs, likely due to the steric hindrance imposed by the bulky nature of BTFE. Meanwhile, the TTE-based MSEs show a coordination structure similar to that of PhF-based MSEs, but with weak $M^{+/2+}$-$O_{(TTE)}$ interactions.

Li^+ creates a strong electrostatic attraction, leading to short interaction distances and tightly bound coordination shells, which also limits the number of ligands, resulting in low CNs. In contrast, Na^+ and K^+, with weaker electrostatic attraction, result in higher CNs, as their coordination shells can accommodate more ligands. In KFSI/TEG electrolytes, K^+ has been shown to reach CNs up to 7 at higher concentrations.[39] Meanwhile, due to its divalent nature, Ca^{2+} exhibits strong electrostatic attraction but yet achieves higher CNs, as its high charge density enables it to attract ligands also at longer distances despite some steric constraints. Katz et al. similarly reported that Ca^{2+} ions in crystal structures favor coordination with oxygen atoms, with CNs of 6 to 8.[40]

2.2. Energy Decomposition and Analysis

From the PMF profiles (**Figure 4**), we find distinct energy minima that correlate with the cation radius. Within each MSE, the sequence of PMF minima follows the order $Li^+ < Ca^{2+} < Na^+ < K^+$, but shifts to higher distances, which indicates weaker cation–anion interactions and less tight coordination for the larger monovalent cations. These trends are consistent with theoretical predictions by Goodwin et al. who demonstrate how cation charge and size govern association energetics and local coordination in concentrated nonaqueous electrolytes.[41] The depth of the PMF minima correlates with the energetic stabilization energy, and across all MSEs, Ca^{2+} exhibits the deepest minimum.

The energy barriers extracted from the PMF profiles (**Figure 5**) quantify the free energy required for cations to escape their coordination shell. The trend in energy barriers follows the charge-to-radius ratio, with Ca^{2+} exhibiting the highest barriers and K^+ the lowest barriers.

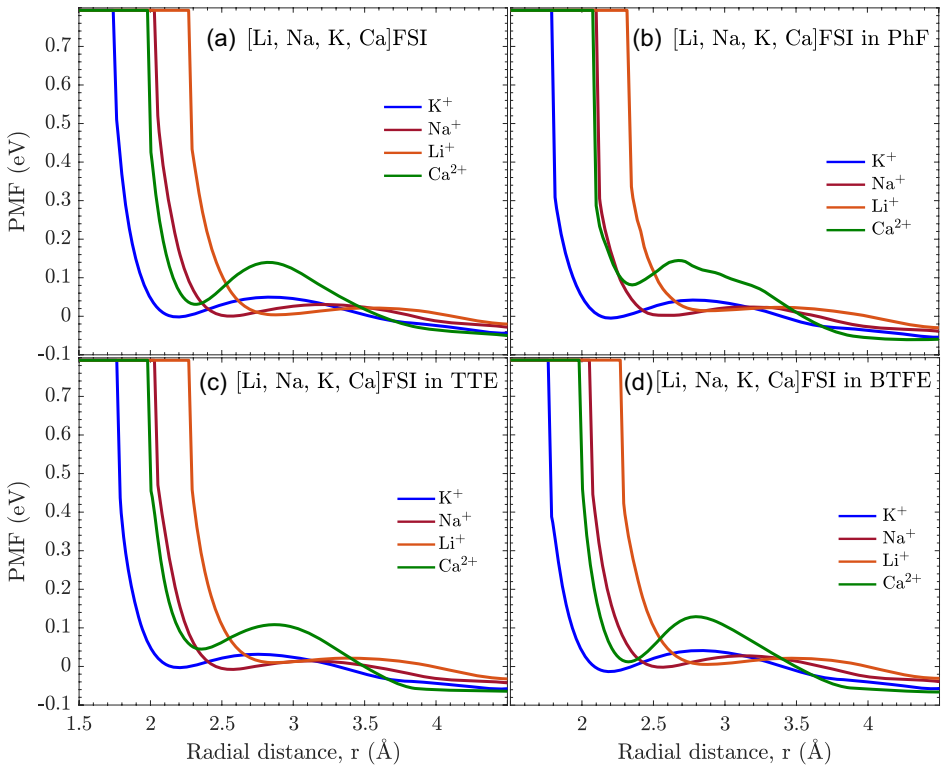

Figure 4. PMFs profiles for Li^+, Na^+, K^+, and Ca^{2+} in a) FSI-, b) FSI-PhF-, c) FSI-TTE-, and d) FSI-BTFE-based MSEs.

Research Article
doi.org/10.1002/batt.202500239
Chemistry Europe
European Chemical Societies Publishing

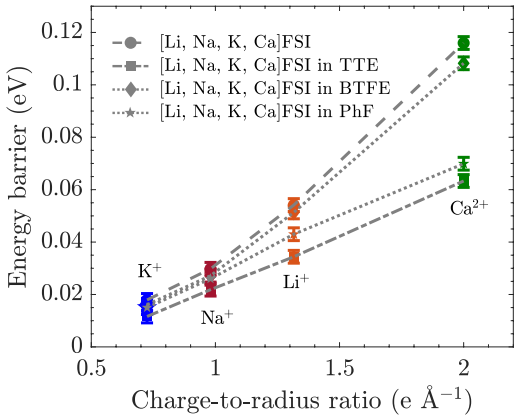

Figure 5. Energy barriers extracted from the PMF profiles for Li^+, Na^+, K^+, and Ca^{2+} in FSI-, FSI-TTE-, FSI-BTFE-, and FSI-PhF-based MSEs.

Among the MSEs with fluorinated additives, the TTE-based one exhibits the largest reduction in energy barriers, which we attribute to TTE's dual effect of directly participating in the cation coordination and allowing for a more compact molecular structure. The PhF-based MSE also has a noticeable energy barrier reduction despite no direct cation coordination by PhF, likely due to charge screening effects. In contrast, BTFE participates in the cation coordination, but its bulkier structure may sterically hinder solvation rearrangements, in total leading to the smallest reduction in energy barriers.

The decomposition of the energy into E_{Coul}, E_{vdW}, and E_{pot} (**Figure 6**-a,b,c) with E_{Coul} scaled down by a factor of 10^3 and E_{pot} by 10^2 for better visual comparison, highlights that E_{Coul} is the dominant contributor to the total interaction energy, while E_{pot} remains negative, ensuring thermodynamic stability.

While the Coulombic forces dominate the total interaction energy in MSEs due to their long-range nature and strong ion–ion interactions, the vdW forces/dispersion interactions, which are weaker but also more short-range, significantly influence the local coordination. The effect of fluorinated solvents/additives, however, extends beyond their contribution to the vdW forces (Figure 6-a); they also physically disrupt the ionic network, thus indirectly weakening the Coulombic interactions (Figure 6-b). BTFE has the largest effect on the former, likely due to its bulkier structure and greater polarizability, while the PhF-based MSE behaves close to the pure FSI-based MSE, and hence the action of a non-coordinating and only spatially disruptive diluent is rather minor. TTE falls between these extremes, balancing participation in the cation coordination with moderate vdW stabilization.

The relative energy differences versus the pure FSI-based MSE as reference (Figure 6-d) reveal that all additive-containing MSEs exhibit a comparable reduction in Coulombic energy, suggesting a similar degree of electrostatic weakening by increased spatial disruption, indicating that the primary mechanism of action is the latter. Still, the distinct vdW contributions are what set them apart.

The E_{pot} differences vary across the MSEs, indicating that while Coulombic interactions are consistently weakened, the overall impact on thermodynamic stability depends on the balance between vdW stabilization and structural reorganization.

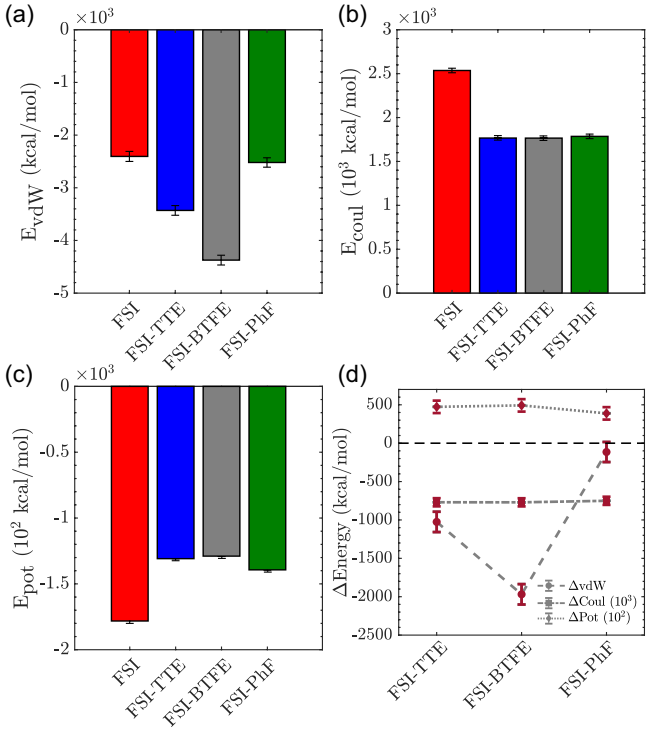

Figure 6. a) Average van der Waals (E_{vdW}), b) Coulombic (E_{coul}), c) total potential (E_{pot}) energies, and d) relative energy differences (ΔEnergy) of van der Waals (ΔvdW), Coulombic (ΔCoul), and potential (ΔPot) energies for FSI-TTE, FSI-BTFE, and FSI-PhF MSEs, calculated with respect to the solvent-free MSE. E_{coul} and E_{pot} are scaled down by factors of 10^3 and 10^2, respectively, to enable visual comparison with E_{vdW}. Error bars represent standard deviations from MD simulations.

2.3. Dynamics Analysis

The MSDs (**Figure 7**-a) reveal that the pure FSI-based MSE shows the slowest diffusion, as expected, characterized by prolonged caging regimes due to strong Coulombic interactions, while fluorinated additives enhance the mobility, as indicated by an increased MSD slope and reduced caging.

Likewise, the total self-diffusion coefficients (Figure 7-b) demonstrate a significant increase, especially for the TTE-based MSE. Again, TTE weakens the ionic interactions without significantly hindering motion, while PhF mainly enhances the mobility through dilution. BTFE, however, creates a more structured solvation shell for the cations, leading to slower diffusion.

The additive diffusion coefficients (Figure 7-c) follow a similar trend, indicating that overall mobility is driven by both cation and additive dynamics. The PhF-based MSE yields the fastest solvent diffusion, due to its non-interacting nature and disruptive effect on the ionic network, while BTFE shows the slowest solvent diffusion, being a bulky molecule.

As for the cation dynamics (Figure 7-d), K^+ and Na^+ have faster diffusion due to weaker Coulombic interactions, while Li^+ and Ca^{2+} diffuse more slowly, due to tighter coordination. Similar diffusion trends linked to cation size and charge have been reported for Li, Na, and K fluoride-based molten salts by Zhang et al..[42] Again, the additives notably improve the cation transport, especially visible for the PhF- and TTE-based MSEs.

Research Article
doi.org/10.1002/batt.202500239
Chemistry Europe
European Chemical Societies Publishing

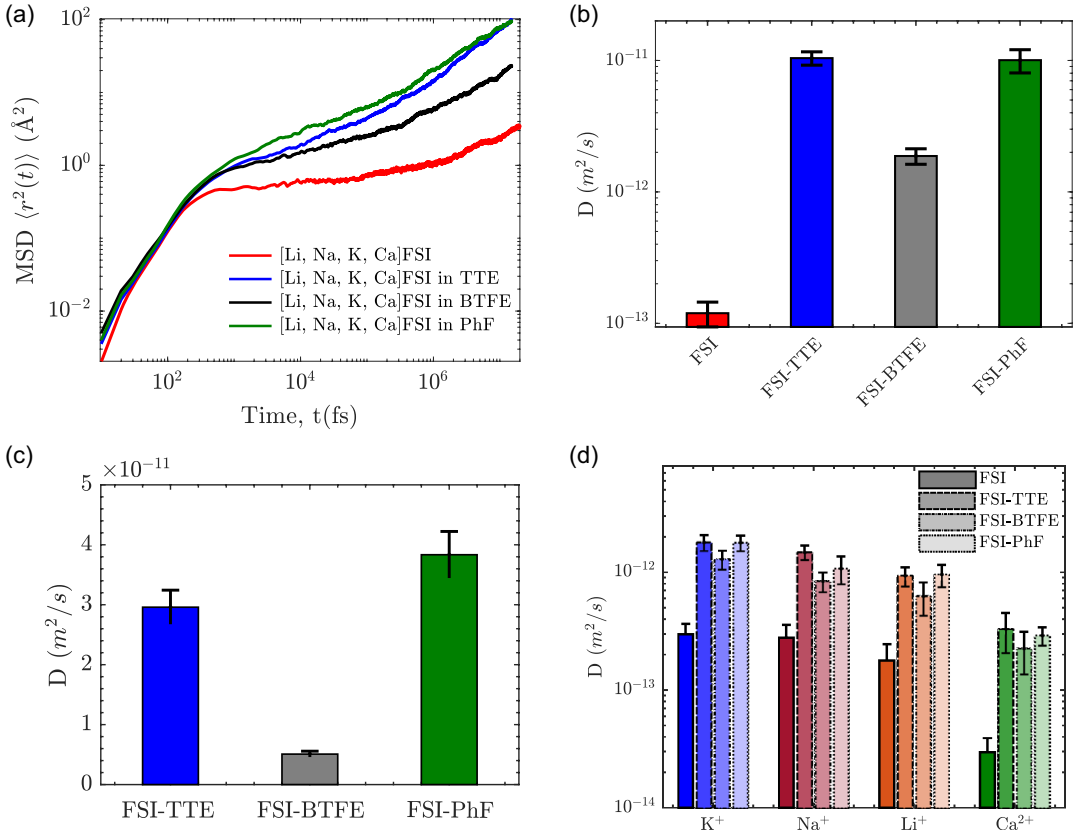

Figure 7. a) MSDs, b) total self-diffusion coefficients, c) solvent self-diffusion coefficients, and d) cations self-diffusion coefficients in FSI-, FSI-TTE-, FSI-BTFE-, and FSI-PhF-based MSEs.

Moving to the cation cage dynamics, the pure FSI-based MSE exhibits the longest CaL, significantly shortened by the additives, with TTE and BTFE behaving similarly, but the PhF-based MSE highlighting PhF's capacity to destabilize the cages through dilution and weaker vdW stabilization.

As for LER (**Figure 8**-right), the pure FSI-MSE exhibits the highest rates, maintaining a dynamic coordination structure. Perhaps unexpectedly, because of the lower Coulombic interactions, both TTE and BTFE lower the LER, which is due to their stabilizing effects on the cation environment, with BTFE imposing slightly more steric constraints. Finally, the PhF-based MSE shows the lowest LER, which reflects its vdW interactions that reduce the ligand-cation dynamics. Åvall & Johansson[43] demonstrated that ligand exchange frequency is modulated by cation identity and coordination strength, with higher salt concentrations favoring more dynamic solvation. Similarly, Åvall et al.[44] reported that

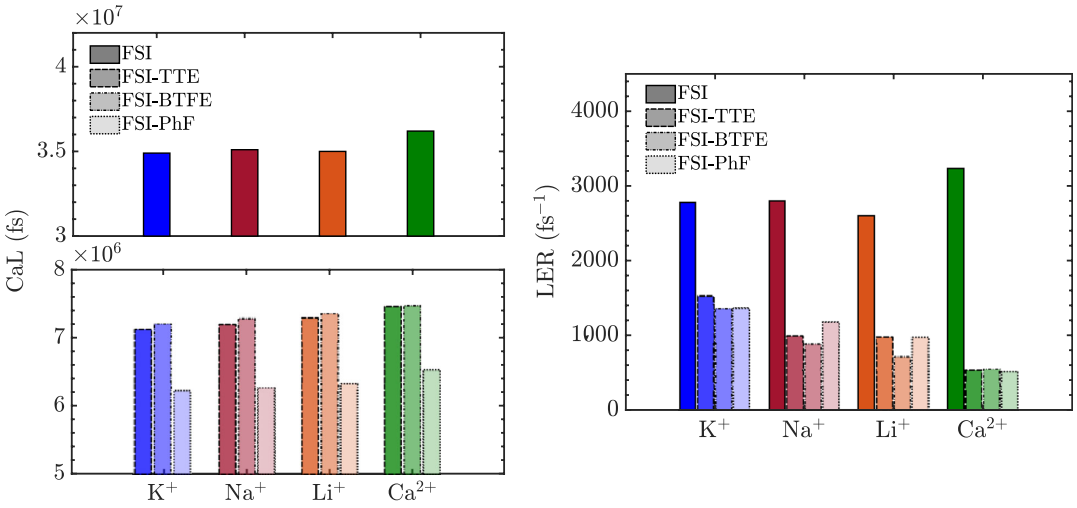

Figure 8. CaL (right) and LER (left) of Li^+, Na^+, K^+ and Ca^{2+} in the FSI-, FSI-TTE-, FSI-BTFE-, and FSI-PhF-based MSEs.

changes in salt content directly impact the solvation shell structure and ligand residence times, aligning with our findings that additives like TTE and PhF affect CaL and LER via coordination disruption and van der Waals stabilization, respectively.

Overall, very distinct LER and CaL trends are observed for each of the cations in all the MSEs, with K^+ exhibiting both the highest LERs and shortest CaLs, suggesting frequent ligand turnover amid shorter shell retention times, together assuring "fast" cation transport. For Ca^{2+}, however, the opposite behavior is observed, with the lowest LERs and the longest CaLs, indicating a much more stable coordination characterized by slow ligand exchange and strong cage persistence. While this implies sluggish transport relative to monovalent cations, such stability may, in fact, be advantageous for CaBs, where strong ion–solvent interactions can contribute to enhanced interfacial stability and selective transport at the electrode–electrolyte interface.[45]

3. Conclusion

Fluorinated additives can modulate the structural and transport properties of MSEs, by providing a molecular-level design strategy to fine-tune ion-ion and ion–solvent interactions, and possibly also alter the MSEs' interfacial properties. The systematic comparison of TTE, BTFE, and PhF in a multicationic FSI-based MSE reveals that differences in steric hindrance, coordination capacity, and van der Waals stabilization lead to distinctly different behaviors, which underscores that additive effects are not merely compositional.

Yet, the targeted Ca^{2+} transport may, however, not benefit from these strategies in a decisive manner as the strong and persistent coordination typically present in the Ca^{2+}-based MSEs prevent fast ligand and cage dynamics, which is needed for the targeted interfacial behavior, a particularly relevant consideration for CaBs, where SEI formation and compatibility remain key challenges. This echoes what was shown by Nguyen & Filhol; Ca^{2+} reduction requires partial desolvation, whereas (too) strong cation coordination suppresses plating and promotes solvent degradation.[46]

Considering all of the above, a more nuanced approach can be adopted when extending MSE engineering to experimentally validated electrolytes, potentially unlocking new pathways toward functional CaBs. These molecular-level insights help identify additive features—such as coordination ability or steric influence—that modulate Ca^{2+} solvation and transport. For example, non-coordinating additives like PhF can dilute the ionic network and weaken van der Waals interactions, enhancing ion mobility but possibly compromising interfacial stability. In contrast, coordinating additives such as BTFE or TTE may slow ligand exchange, yet support more stable solvation shells and SEI formation. Balancing these effects, by tuning additive ratios or combining diluent types, could offer a viable strategy to optimize Ca^{2+} plating efficiency and long-term battery performance.

While this study focuses on bulk-phase electrolyte behavior, performance in real cells is strongly influenced by interfacial phenomena. Ion solvation and additive effects can shift dramatically near electrode surfaces due to altered coordination environments and potential-dependent reactivity. For instance, Song et al. demonstrated that a hybrid SEI can enable ultralong-life calcium-metal batteries by stabilizing the interface and suppressing dendrite growth.[47] Similarly, He et al. reported that a compact nitrogen-rich interphase layer facilitates reversible calcium-metal chemistry in commercial fluorinated calcium salt ester electrolytes at room temperature.[48] These findings underscore the importance of future studies that integrate bulk electrolyte insights with interfacial modeling and experiments to enable practical CaB technologies.

4. Computational Approach and Analysis

MD simulations were performed using the LAMMPS software package[49] and the CL&Pol polarizable force field.[50–53] Cubic simulation boxes containing 1575 molecules - comprising 140 of each of the cations (Li^+, Na^+, K^+, and Ca^{2+}), 700 FSI anions, and 315 solvent molecules (TTE, BTFE, or PhF), corresponding to *ca.* 40, 40, and 20 wt%—were constructed using the *Packmol* software.[54] The molecular topology files, Lennard-Jones parameters, and bonded parameters were generated with the *fftool* package.[55]

An initial energy minimization was performed using the conjugate gradient method, followed by a series of equilibration steps. The electrolytes were equilibrated at 400 K under the isothermal-isobaric ensemble (NPT) at 1 atm for 3 ns. This was followed by two equilibration steps in the canonical ensemble (NVT), consisting of a 3 ns run and an additional 5 ns run.

Production runs were conducted in the NVT ensemble using the average simulation box size obtained from the NPT equilibration runs. These production runs were performed for 28 ns. A Nosé-Hoover thermostat was applied with a temperature damping constant of 100 fs and a pressure damping constant of 1000 fs. Electrostatic interactions were calculated using the particle–particle particle-mesh (PPPM) method, and periodic boundary conditions were applied in all directions.

Structural analysis was carried out by computing radial distribution functions (RDFs) and coordination numbers (CNs) using LAMMPS subroutines. To further assess the thermodynamic stability of cation–anion interactions, potential of mean force (PMF) profiles were derived from the RDFs using the relationship $PMF(r) = -k_BT \ln g(r)$, where k_B is the Boltzmann constant and T is the simulation temperature. The PMF provides insights into the strength and spatial extent of cation–anion interactions, with deeper minima corresponding to stronger electrostatic interactions. Additionally, energy barriers were extracted from the PMF profiles to quantify the free energy required for cations to escape the first coordination shell, serving as a measure of coordination stability. Finally, the energy values were extracted from the LAMMPS log files, averaged over the production trajectory, and decomposed into Coulombic (E_{Coul}), van der Waals (E_{pvdW}), and total potential energy (E_{pot}) contributions.

Dynamic properties were assessed by calculating the mean square displacement (MSD) and extracting self-diffusion coefficients based on the Einstein relation.[56] Two complementary

metrics were computed to evaluate the influence of the solvents on cage dynamics: the cage lifetime (CaL) and the ligand exchange rate (LER).

CaL is the average time a cation remains "caged" or structurally restricted by surrounding anions or solvent molecules, that is, measures the persistence of the cage itself and is defined by the integral of the cage autocorrelation function (CAF) over time.[57] In contrast, the LER quantifies the frequency by which the cation's coordination shell is altered and is calculated as the total number of exchange events divided by the total simulation time, that is, the rate of ligand turnover.[43] Using both measures, calculated using trajectory data and custom Python scripts, for each of the cations separately, is important as a high LER does not necessarily imply disintegration of the cage, but this is captured by the CaL metric.

Acknowledgements

The authors would like to acknowledge the financial support from the Swedish Research Council (grants #2020 – 03988 and #2021 – 00613) and VINNOVA/Batteries Sweden (BASE) (grant 2019-00064). The authors also thank Dr. Patricia Huijbers for her valuable insights and feedback during the preparation of this manuscript.

Conflict of Interest

The authors declare no conflict of interest.

Data Availability Statement

The data that support the findings of this study are available from the corresponding author upon reasonable request.

Keywords: calcium batteries · cation coordination · fluorinated additives · molecular dynamics simulations · molten salt electrolytes

[1] B. Vedhanarayanan, K. Seetha Lakshmi, *Front. Batteries Electrochem.* **2024**, *3*, 1377192.
[2] J. Zhang, X. Yao, R. K. Misra, Q. Cai, Y. Zhao, *J. Mater. Sci. Technol.* **2020**, *44*, 237.
[3] Q. Wei, L. Zhang, X. Sun, T. L. Liu, *Chem. Sci.* **2022**, *13*, 5797.
[4] A. K. Tan, S. Paul, *Energies* **2024**, *17*, 5768.
[5] A. Ponrouch, J. Bitenc, R. Dominko, N. Lindahl, P. Johansson, M. Palacín, *Energy Storage Mater.* **2019**, *20*, 253.
[6] M. R. Palacín, P. Johansson, R. Dominko, B. Dlugatch, D. Aurbach, Z. Li, M. Fichtner, O. Lužanin, J. Bitenc, Z. Wei, C. Glaser, J. Janek, A. Fernández-Barquín, A. R. Mainar, O. Leonet, I. Urdampilleta, J. A. Blázquez, D. S. Tchitchekova, A. Ponrouch, P. Canepa, G. S. Gautam, R. S. R. G. Casilda, C. S. Martinez-Cisneros, N. U. Torres, A. Varez, J.-Y. Sanchez, K. V. Kravchyk, M. V. Kovalenko, A. A. Teck, H. Shiel, I. E. L. Stephens, M. P. Ryan, E. Zemlyanushin, S. Dsoke, R. Grieco, N. Patil, R. Marcilla, X. Gao, C. J. Carmalt, G. He, M.-M. Titirici, *J. Phys.: Energy* **2024**, *6*, 031501.
[7] Y. Liang, H. Dong, D. Aurbach, Y. Yao, *Nat. Energy* **2020**, *5*, 646.
[8] L. Wang, S. Riedel, Z. Zhao-Karger, *Adv. Energy Mater.* **2024**, *14*, 2402157.
[9] H. Lin, J. Meng, W. Guo, R. Li, Y. Yi, Y. Ma, C. F. Cheung, D. Aurbach, Z.-L. Xu, *Energy Environ. Sci.* **2024**, *17*, 6548.
[10] D. Wang, X. Gao, Y. Chen, L. Jin, C. Kuss, P. G. Bruce, *Nat. Mater.* **2018**, *17*, 16.
[11] Z. Li, O. Fuhr, M. Fichtner, Z. Zhao-Karger, *Energy Environ. Sci.* **2019**, *12*, 3496.
[12] J. Timhagen, C. Cruz, J. Weidow, P. Johansson, *Batteries Supercaps* **2024**, *7*, e202400297.
[13] S. Yan, N. Yao, H. Liu, Z. Zhang, Y. Lu, Z. Liu, W. Hou, P. Zhou, H. Zhou, X. Chen, K. Liu, Q. Zhang, *Energy Environ. Sci.* **2025**, *18*, 1696.
[14] H. Liu, X. Zhang, S. He, D. He, Y. Shang, H. Yu, *Mater. Today* **2022**, *60*, 128.
[15] M. Kerner, N. Plylahan, J. Scheers, P. Johansson, *Phys. Chem. Chem. Phys.* **2015**, *17*, 19569.
[16] M. Kerner, N. Plylahan, J. Scheers, P. Johansson, *Rsc Adv.* **2016**, *6*, 23327.
[17] H.-B. Han, S.-S. Zhou, D.-J. Zhang, S.-W. Feng, L.-F. Li, K. Liu, W.-F. Feng, J. Nie, H. Li, X.-J. Huang, M. Armand, Z.-B. Zhou, *J. Power Sources* **2011**, *196*, 3623.
[18] S. Roy, F. Wu, H. Wang, A. S. Ivanov, S. Sharma, P. Halstenberg, S. K. Gill, A. M. Milinda Abeykoon, G. Kwon, M. Topsakal, B. Layne, K. Sasaki, Y. Zhang, S. M. Mahurin, S. Dai, C. J. Margulis, E. J. Maginn, V. S. Bryantsev, *Phys. Chem. Chem. Phys.* **2020**, *22*, 22900.
[19] S. Roy, M. Brehm, S. Sharma, F. Wu, D. S. Maltsev, P. Halstenberg, L. C. Gallington, S. M. Mahurin, S. Dai, A. S. Ivanov, C. J. Margulis, V. S. Bryantsev, *J. Phys. Chem. B* **2021**, *125*, 5971.
[20] M. McEldrew, Z. A. H. Goodwin, N. Molinari, B. Kozinsky, A. A. Kornyshev, M. Z. Bazant, *J. Phys. Chem. B* **2021**, *125*, 13752-13766.
[21] D. Zhao, L. Yan, T. Jiang, S. Peng, B. Yue, *J. Energy Storage* **2023**, *61*, 106707.
[22] H. P. K. Ngo, E. Planes, C. Iojoiu, P. Soudant, A.-L. Rollet, P. Judeinstein, *J. Ionic Liquids* **2022**, *2*, 100044.
[23] S. Perez Beltran, X. Cao, J.-G. Zhang, P. Z. El-Khoury, P. B. Balbuena, *J. Mater. Chem. A* **2021**, *9*, 17459.
[24] J. Li, S. Sui, X. Zhou, K. Lei, Q. Yang, S. Chu, L. Li, Y. Zhao, M. Gu, S. Chou, S. Zheng, *Angew. Chem. Int. Ed.* **2024**, *63*, e202400406.
[25] H. A. Ishfaq, C. Cruz Cardona, E. Tchernychova, P. Johansson, R. Dominko, S. Drvarič, Talian, *Energy Storage Mater.* **2024**, *69*, 103375.
[26] H. Jia, J. Kim, P. Gao, Y. Xu, M. H. Engelhard, B. E. Matthews, C. Wang, W. Xu, *Angew. Chem.* **2023**, *135*, e202218005.
[27] W. van Ekeren, A. Hall, K. Lahtinen, R. Younesi, *ChemElectroChem* **2024**, *11*, 1.
[28] Y. Wang, Z. Li, Y. Hou, Z. Hao, Q. Zhang, Y. Ni, Y. Lu, Z. Yan, K. Zhang, Q. Zhao, F. Li, J. Chen, *Chem. Soc. Rev.* **2023**, *52*, 2713.
[29] W. W. A. van Ekeren, M. Albuquerque, G. Ek, R. Mogensen, W. R. Brant, L. T. Costa, D. Brandell, R. Younesi, *J. Mater. Chem. A* **2023**, *11*, 4111.
[30] N. T. Hahn, J. Self, D. M. Driscoll, N. Dandu, K. S. Han, V. Murugesan, K. T. Mueller, L. A. Curtiss, M. Balasubramanian, K. A. Persson, K. R. Zavadil, *Phys. Chem. Chem. Phys.* **2022**, *24*, 674.
[31] Y. Zhao, T. Zhou, T. Ashirov, M. E. Kazzi, C. Cancellieri, L. P. H. Jeurgens, J. W. Choi, A. Coskun, *Nat. Commun.* **2022**, *13*, 2575.
[32] X. Cao, P. Gao, X. Ren, L. Zou, M. H. Engelhard, B. E. Matthews, J. Hu, C. Niu, D. Liu, B. W. Arey, C. Wang, J. Xiao, J. Liu, W. Xu, J.-G. Zhang, *Proc. Natl. Acad. Sci.* **2021**, *118*,e2020357118.
[33] Y. Zhao, T. Zhou, M. Mensi, J. W. Choi, A. Coskun, *Nat. Commun.* **2023**, *14*, 299.
[34] Y. Yi, Y. Xing, H. Wang, Z. Zeng, Z. Sun, R. Li, H. Lin, Y. Ma, X. Pu, M. M. Li, K. Park, Z. Xu, *Angew. Chem. Int. Ed.* **2024**, *63*, e202317177.
[35] S. Biria, S. Pathreeker, I. D. Hosein, *ChemRxiv* **2021**, preprint, DOI: 10.26434/chemrxiv-2021-djssr.
[36] H. A. Ishfaq, C. Cruz Cardona, E. Tchernychova, P. Johansson, M. Gaberšček, R. Dominko, S. Drvarič Talian, *Chem. Mater.* **2025**, *37*, 2485.
[37] X. Li, X. Wu, H. A. Doan, Z. Yang, R. Amine, M. Li, M. V. Bracamonte, C.-C. Su, K. Amine, *ACS Energy Lett.* **2024**, *9*, 3484.
[38] Z. Jiang, Z. Zeng, B. Zhai, X. Li, W. Hu, H. Zhang, S. Cheng, J. Xie, *J. Power Sources* **2021**, *506*, 230086.
[39] L. C. Meyer, P. Johansson, A. Balducci, *ChemPhysChem* **2024**.
[40] A. K. Katz, J. P. Glusker, S. A. Beebe, C. W. Bock, *J. Am. Chem. Soc.* **1996**, *118*, 5752.
[41] Z. A. Goodwin, M. McEldrew, B. Kozinsky, M. Z. Bazant, *PRX Energy* **2023**, *2*, 013007.
[42] W. Zhang, X. Hu, H. Kang, R. Guo, J. Yu, Z. Wang, *J. Phys. Chem. B* **2025**, *129*, 2246.
[43] G. Åvall, P. Johansson, *J. Chem. Phys.* **2020**, *152, 234104*.
[44] G. Åvall, J. Wallenstein, G. Cheng, K. L. Gering, P. Johansson, D. P. Abraham, *J. Electrochem. Soc.* **2021**, *168*, 050521.
[45] S. S. R. K. C. Yamijala, H. Kwon, J. Guo, B. M. Wong, *ACS Appl. Mater. Interfaces* **2021**, *13*, 13114.
[46] L. H. B. Nguyen, J. Filhol, *Adv. Energy Mater.* **2023**, *13*, 2300311.
[47] H. Song, J. Su, C. Wang, *Adv. Mater* **2021**, *33*, 2006141.
[48] X. He, F. Tian, H. Song, C. Wang, *Chem. Eng. J.* **2024**, *502*, 157793.

[49] S. Plimpton, *J. Comput. Phys.* **1995**, *117*, 1.
[50] K. Goloviznina, Z. Gong, M. F. Costa Gomes, A. A. Pádua, *J. Chem. Theory Comput.* **2021**, *17*, 1606-1617.
[51] K. Goloviznina, J. N. Canongia Lopes, M. Costa Gomes, A. A. H. Pádua, *J. Chem. Theory Comput.* **2019**, *15*, 5858.
[52] R. Maglia de Souza, M. Karttunen, M. C. C. Ribeiro, *J. Chem. Inf. Model.* **2021**, *61*, 5938.
[53] K. Goloviznina, Z. Gong, A. A. H. Pádua, *WIREs Comput. Mol. Sci.* **2022**, *12*, e1572.
[54] L. Martínez, R. Andrade, E. G. Birgin, J. M. Martínez, *J. Comput. Chem.* **2009**, *30*, 2157.
[55] A. A. H. Pádua, *J. Chem. Phys.* **2017**, *146, 204501*.
[56] D. Frenkel, B. Smit, *Understanding Molecular Simulation: From Algorithms to Applications*, Elsevier **2023**.
[57] M. Sha, X. Ma, N. Li, F. Luo, G. Zhu, M. D. Fayer, *J. Chem. Phys.* **2019**, *151*, 154502.

Manuscript received: March 31, 2025
Revised manuscript received: May 15, 2025
Version of record online: June 10, 2025